# Contents:

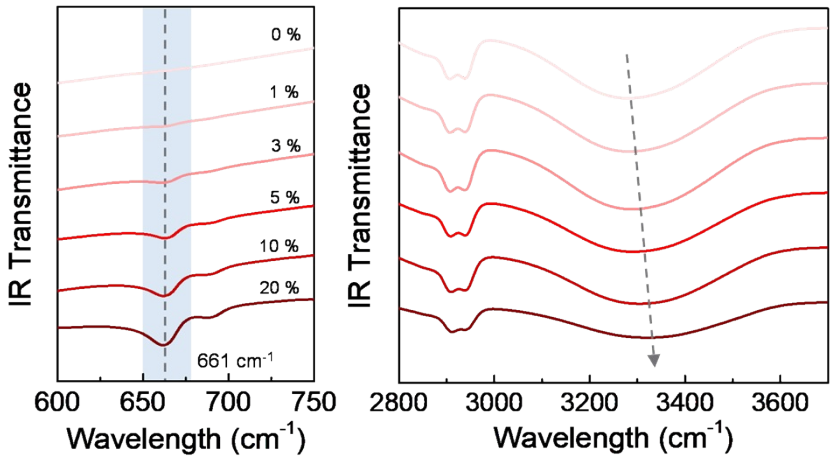


**Figue S1. Fourier transform infrared transmission spectra of the films.** Fourier transform infrared transmission spectra of PVA and *c*PVA films with different ratios of crosslinker (boric acid, 1%, 3%, 5%, 10% and 20%). The wavenumber bands centered at 661 $cm^{-1}$ and 3300 $cm^{-1}$ correspond B-O group and -OH group respectively.

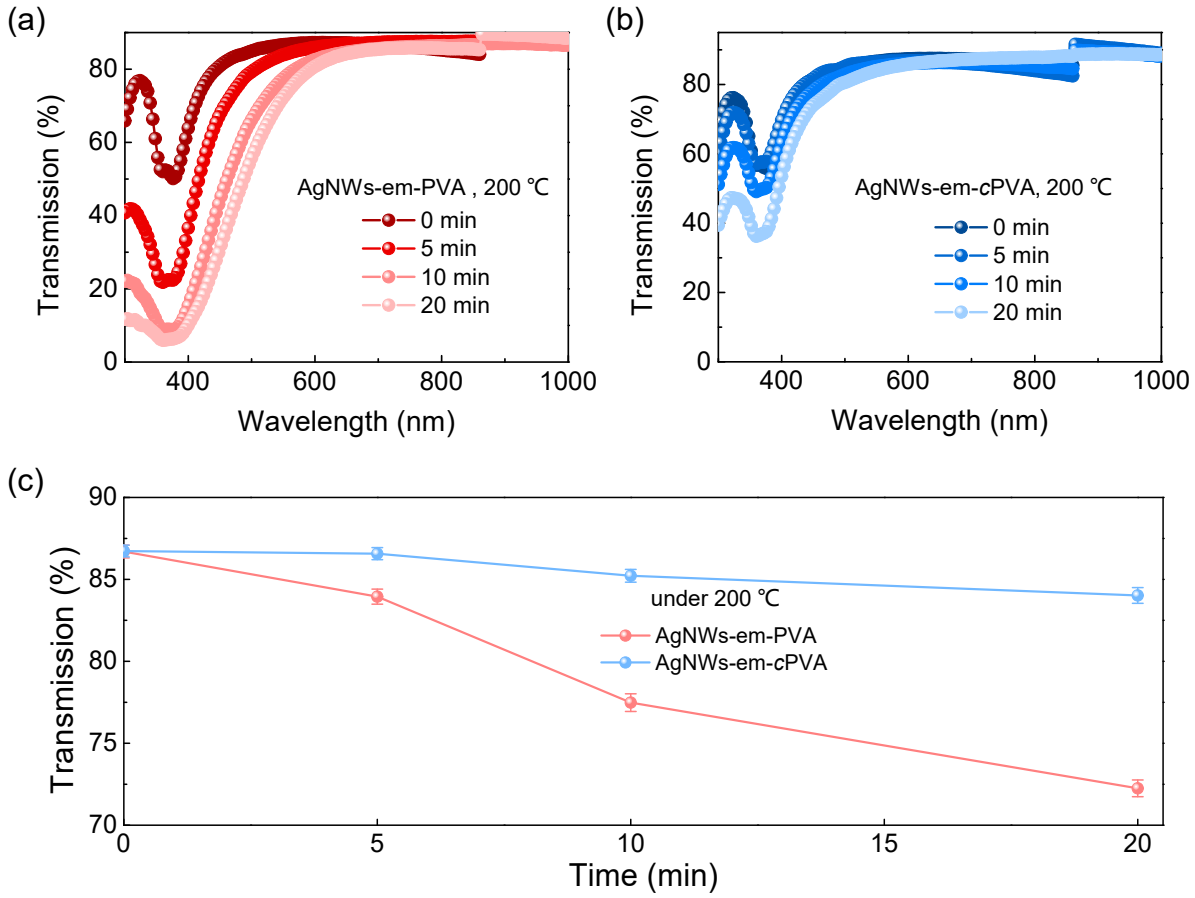


**Figure S2. The transmission of the electrodes after annealed at 200 ℃ for different times.** The transmission of the AgNWs-em-PVA (a) and AgNWs-em-*c*PVA (b) electrodes after annealed at 200 ℃ for 0 min, 5 min, 10 min and 20 min. (c) The transmission at 550 nm of AgNWs-em-PVA and AgNWs-em-*c*PVA electrodes after annealed at 200°C for different durations. Data are presented as mean values ± standard deviation over 10 samples for each electrode. Curves drawn on top of data are guides to the eye.

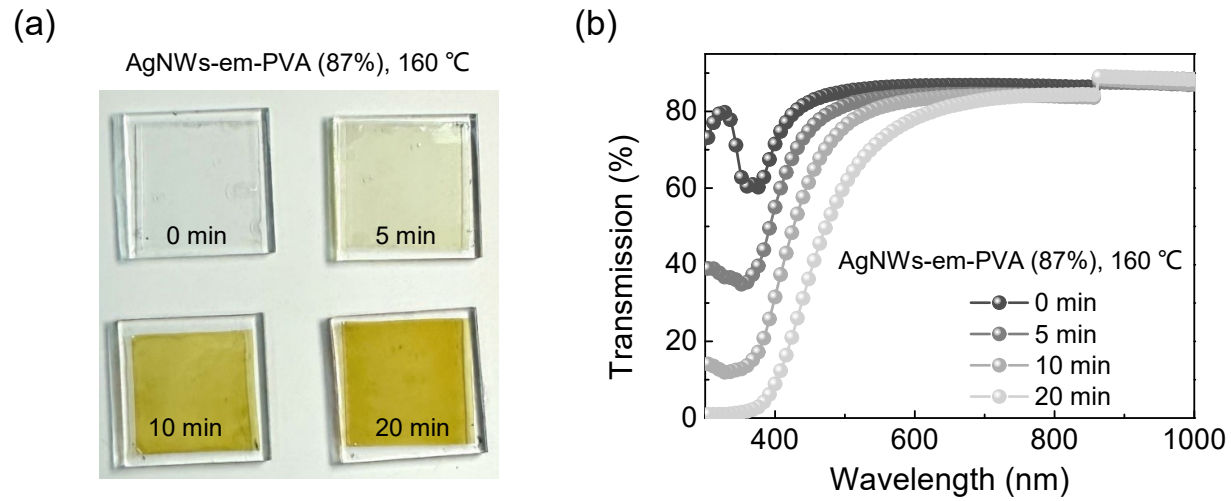


**Figure S3. The changes in color and transmittance of the electrodes after annealed at 160 ℃ for different times.** Photos of color changes (a) and transmittance (b) of the AgNWs-em-PVA (87%) electrodes after annealed at 160 ℃ for 0 min, 5 min, 10 min and 20 min. Curves drawn on top of data are guides to the eye.


**Figure S4. The photos of the electrodes used for testing moisture adsorption rate.** The electrode of the AgNWs-em-PVA (87%), AgNWs-em-PVA and AgNWs-em-*c*PVA electrodes, with dimensions of 9.5 cm × 9.5 cm, were adhered to glass/PDMS substrates and exposed in an environment with a humidity of 60% and a temperature of 25 ℃.

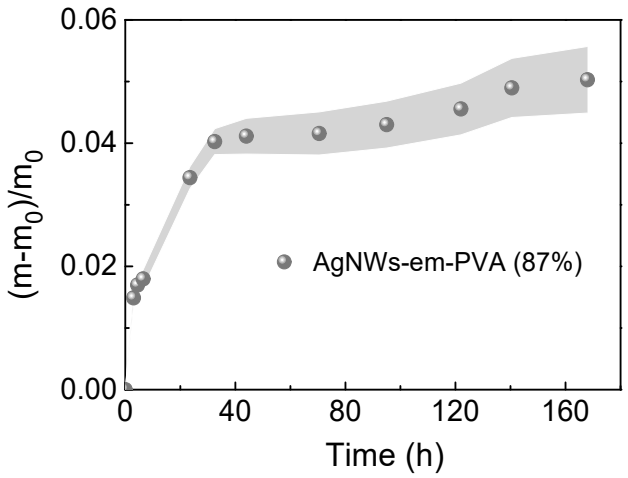


**Figure S5. The moisture adsorption rate of the electrodes.** The rate of change in the AgNWs-em-PVA (87%) electrode mass (calculated as the difference between real-time mass and initial mass, divided by the initial mass) varies with the duration of placement. Data are presented as mean values ± standard deviation over 10 samples. Curves drawn on top of data are guides to the eye.

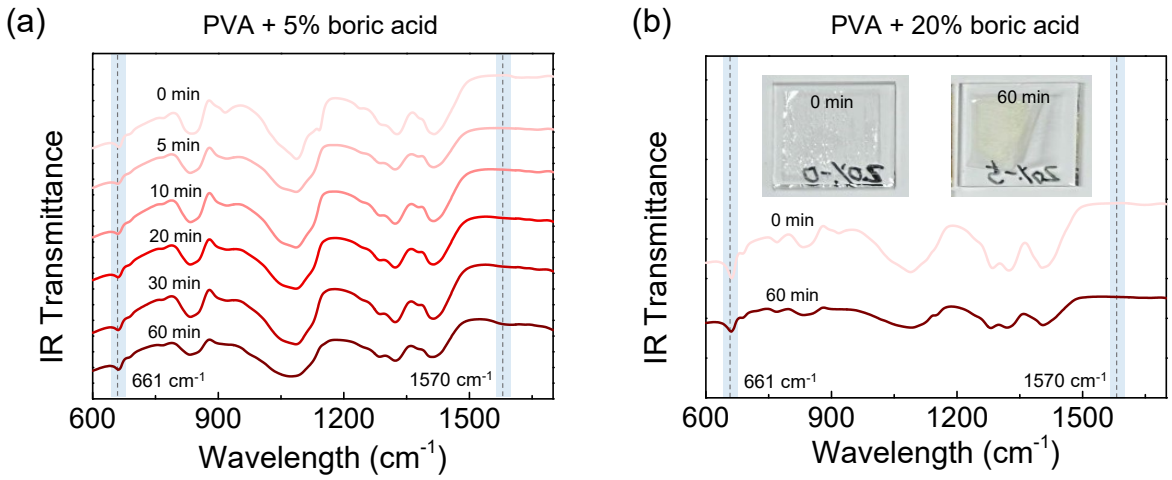


**Figure S6. Fourier transform infrared transmission spectrum of the *c*PVA.** Fourier transform infrared transmission spectrum of *c*PVA films with crosslinking degree of 5% (b) and 20% (b). The inset in (b) shows photographs of a 20% crosslinked PVA film before and after annealing at 200 °C for 60 minutes. Curves drawn on top of data are guides to the eye.

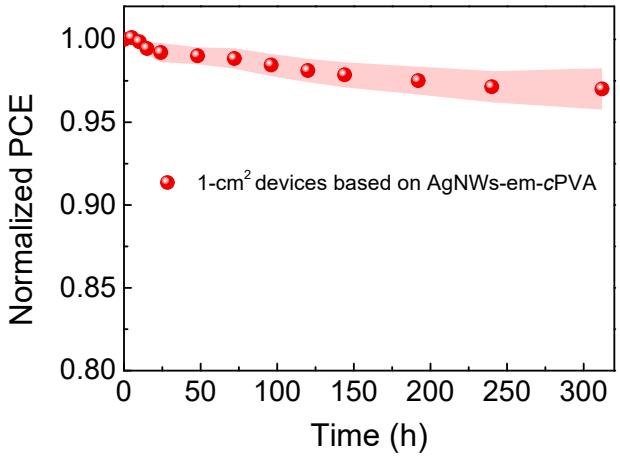


**Figure S7. Thermal stability of 1-cm² flexible devices based on AgNWs-em-*c*PVA electrodes at 80 °C in a $N_2$-filled glovebox.** Data are presented as mean values ± standard deviation over 10 samples. Curves drawn on top of data are guides to the eye.

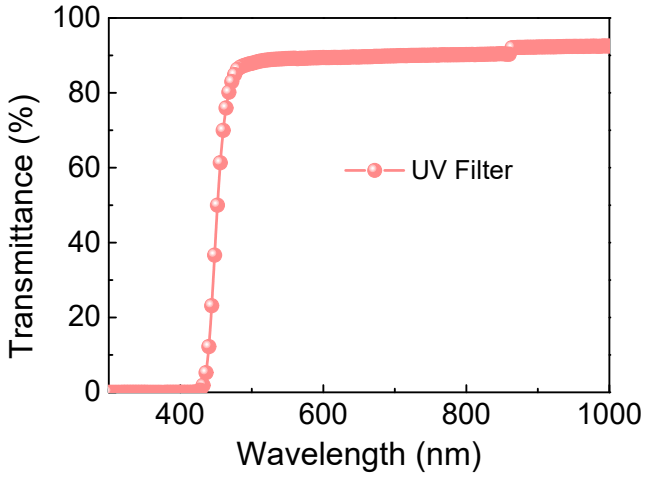


**Figure S8. The transmittance of the UV filter with the wavelength from 300 nm to 1,000 nm.** Curves drawn on top of data are guides to the eye.

**Table S1.** Photovoltaic parameters of flexible OSCs (active area: 1 $cm^2$) based on the AgNWs-em-PVA and AgNWs-em-*c*PVA electrodes after being exposed in air with a R.H. of 60% and temperature of 25 °C for different time. The configuration of flexible OSCs is AgNWs-em-PVA or AgNWs-em-*c*PVA/PEI-Zn/PM6:BTP-eC9:$PC_{71}BM$/$MoO_3$/Ag.

| Substrate | Placement time | $V_{OC}$ (V) | $J_{SC}$ ($mA/cm^2$) | FF | PCE (%) |
|---|---|---|---|---|---|
| AgNWs-em-PVA | 0 h | 0.84 | 25.27 | 0.76 | 16.27 (16.11 ± 0.14)[a] |
| | 24 h | 0.84 | 25.19 | 0.73 | 15.27 (15.18 ± 0.25) [a] |
| | 96 h | 0.83 | 25.13 | 0.68 | 14.24 (14.08 ± 0.38) [a] |
| | 168 h | 0.83 | 25.09 | 0.65 | 13.47 (13.41 ± 0.49) [a] |
| AgNWs-em-*c*PVA | 0 h | 0.84 | 25.32 | 0.77 | 16.38 (16.27 ± 0.13) [a] |
| | 24 h | 0.84 | 25.29 | 0.76 | 16.14 (16.07 ± 0.15) [a] |
| | 96 h | 0.84 | 25.27 | 0.76 | 16.11 (16.04 ± 0.18) [a] |
| | 168 h | 0.84 | 25.31 | 0.75 | 15.92 (15.89 ± 0.19) [a] |

[a]Data are presented as mean values ± standard deviation from 15 devices.

**Table S2.** Photovoltaic parameters of flexible OSCs (active area: 1 $cm^2$) based on the AgNWs-em-PVA or AgNWs-em-*c*PVA electrodes with the annealing temperature of the electron transport layer at 200 ℃. The configuration of flexible OSCs is AgNWs-em-PVA/PEI-Zn/PM6:BTP-eC9:$PC_{71}BM$/$MoO_3$/Ag.

| Substrate | $V_{OC}$ (V) | $J_{SC}$ ($mA/cm^2$) | FF | PCE (%) |
|---|---|---|---|---|
| AgNWs-em-PVA | 0.84 | 23.14 | 0.72 | 14.07 (13.97 ± 0.11)[a] |
| AgNWs-em-*c*PVA | 0.84 | 25.26 | 0.76 | 16.13 (16.08 ± 0.12)[a] |

[a]Data are presented as mean values ± standard deviation from 15 devices.

**Table S3.** Summary of the efficiency of flexible large-area modules prepared based on non-ITO electrodes.

| Year | Device structure | Area / $cm^2$ | PCE / % |
|---|---|---|---|
| 2011 | PET/Cr/Al/Cr/P3HT:PCBM/PEDOT:PSS/Au-grid | 13.2 | 2.2 [1] |
| 2012 | PET/Ag/ZnO/P3HT:PCBM/PEDOT:PSS/Ag | 35.5 | 0.44 [2] |
| 2014 | Ag grid&HC PEDOT:PSS/ZnO/MH301:PCBM/PFN/PEDOT:PSS(HTL)/ZnO/MH306:PCBM/PFN/PEDOT:PSS(HTL)/HC PEDOT:PSS&Ag grid | 52.2 | 1.76 [3] |
| 2015 | PET/Cr/Al/Cr/P3HT:PCBM/PEDOT:PSS/Ag Grid | 32.55 | 1.78 [4] |
| | | 6.10 | 2.72 [4] |
| 2019 | Embedded silver grid substrate/PEDOT:PSS/ZnO/P3HT:PCBM/PEDOT:PSS/Ag | 36 | 1.84 [5] |
| 2020 | PET/Ag-grid/PEDOT:PSS/ZnO/PTB7-Th:COi8DFIC:PCBM/$MoO_3$/Ag | 25 | 10.09 [6] |
| | | 50 | 9.05 [6] |
| 2022 | PET/Ag-grid/PEDOT:PSS/ZnO/PM6:Qx-1/$MoO_3$/Ag | 30 | 12.2 [7] |
| 2023 | PET/Ag-grid/PEDOT:PSS/ZnO/AL/$MoO_3$/Ag | 30 | 13.08 [8] |
| 2023 | PET/Ag/PEI-Zn/PM6:BTP-eC9/PEDOT:F/AgNWs-polymer | 21 | 12.3 [9] |
| 2023 | PET/Ag-grid/PEDOT:PSS/ZnO/AL/$MoO_3$/Ag | 46.2 | 13.25 [10] |
| 2024 | AgNWs-em-PVA/PEI-Zn/PM6:BTP-eC9:$PC_{71}BM$/$MoO_3$/Ag | 41 | 14.04 [11] |
| this work | AgNWs-em-*c*PVA/PEI-Zn/PM6:BTP-eC9:$PC_{71}BM$/$MoO_3$/Ag | 52.3 | 14.78 |

## Reference


1. B. Zimmermann, H. F. Schleiermacher, M. Niggemann and U. Würfel, *Sol. Energy Mater. Sol. Cells*, 2011, **95**, 1587-1589.
2. D. Angmo, M. Hösel and F. C. Krebs, *Sol. Energy Mater. Sol. Cells*, 2012, **107**, 329-336.
3. T. R. Andersen, H. F. Dam, M. Hosel, M. Helgesen, J. E. Carle, T. T. Larsen-Olsen, S. A. Gevorgyan, J. W. Andreasen, J. Adams, N. Li, F. Machui, G. D. Spyropoulos, T. Ameri, N. Lemaitre, M. Legros, A. Scheel, D. Gaiser, K. Kreul, S. Berny, O. R. Lozman, S. Nordman, M. Valimaki, M. Vilkman, R. R. Sondergaard, M. Jorgensen, C. J. Brabec and F. C. Krebs, *Energy Environ. Sci.*, 2014, **7**, 2925-2933.
4. D. Kaduwal, H.-F. Schleiermacher, J. Schulz-Gericke, S. Schiefer, Y. Liang Tan, J. Zhang, B. Zimmermann and U. Würfel, *Sol. Energy Mater. Sol. Cells*, 2015, **136**, 200-205.
5. S.-W. Kwak, S.-M. Yoon, S.-M. Yu, Y. Ju and D. Kim, *Sol. Energy Mater. Sol. Cells*, 2019, **193**, 169-177.
6. G. Wang, J. Zhang, C. Yang, Y. Wang, Y. Xing, M. A. Adil, Y. Yang, L. Tian, M. Su, W. Shang, K. Lu, Z. Shuai and Z. Wei, *Adv. Mater.*, 2020, **32**, 2005153.
7. Y.-F. Shen, H. Zhang, J. Zhang, C. Tian, Y. Shi, D. Qiu, Z. Zhang, K. Lu and Z. Wei, *Adv. Mater.*, 2023, **35**, 2209030.
8. C. Tian, J. Zhang, Y. Shen, H. Zhang, Z. Zhang, D. Qiu, L. Zhang and Z. Wei, *Sol. RRL*, 2023, **7**, 2300349.
9. C. Xie, Y. Liu, W. Wei and Y. Zhou, *Adv. Funct. Mater.*, 2023, **33**, 2210675.
10. C. X. Wang, X. M. Ma, Y. F. Shen, D. Deng, H. Zhang, T. Wang, J. Q. Zhang, J. Li, R. Wang, L. L. Zhang, Q. Cheng, Z. Q. Zhang, H. Q. Zhou, C. Y. Tian and Z. X. Wei, *Joule*, 2023, **7**, 2386-2401.
11. X. Lu, C. Xie, Y. Liu, H. Zheng, K. Feng, Z. Xiong, W. Wei and Y. Zhou, *Nat. Energy*, 2024, **9**, 793-802.